Kousar, H. Sajida; Srivastava, Divya; Karppinen, Maarit; Tewari, Girish C.

# Tunable Low-Temperature Thermoelectric Transport Properties in Layered $CuCr(S_{1-x}Se_x)_2$ System

*Published in:*
Zeitschrift fur Anorganische und Allgemeine Chemie

*DOI:*
10.1002/zaac.202300079

Published: 17/07/2023

*Document Version*
Publisher's PDF, also known as Version of record

*Please cite the original version:*
Kousar, H. S., Srivastava, D., Karppinen, M., & Tewari, G. C. (2023). Tunable Low-Temperature Thermoelectric Transport Properties in Layered $CuCr(S_{1-x}Se_x)_2$ System. *Zeitschrift fur Anorganische und Allgemeine Chemie*, *649*(14), Article e202300079. https://doi.org/10.1002/zaac.202300079

Journal of Inorganic and General Chemistry
ZAAC
Zeitschrift für anorganische und allgemeine Chemie

www.zaac.wiley-vch.de

RESEARCH ARTICLE

Check for updates

DOI: 10.1002/zaac.202300079

Special Collection

# Tunable Low-Temperature Thermoelectric Transport Properties in Layered $CuCr(S_{1-x}Se_x)_2$ System

H. Sajida Kousar,[a] Divya Srivastava,[a] Maarit Karppinen,*[a] and Girish C Tewari*[a]

*Dedicated to Prof. Antoine Maignan on the Occasion of his 60th Birthday*

We have characterized the layered $CuCr(S,Se)_2$ system for the spin-polarized electronic band structures and low-temperature thermoelectric transport properties. The electronic band structure calculations reveal semiconducting behavior for $CuCrS_2$, $CuCr(S_{0.5}Se_{0.5})_2$ and $CuCrSe_2$ with an indirect bandgap of 0.42, 0.30 and 0.10 eV, respectively. The systematically decreased bandgap with increasing Se content is in line with the experimental observations showing a semiconductor-to-metal transition with increasing Se-substitution level in the $CuCr(S_{1-x}Se_x)_2$ system because of an increase in the charge carrier density. The *p*-type Seebeck coefficient shows a linear temperature dependence for the samples, like in degenerate semiconductors or metals. The remarkably large Seebeck coefficient even in metallic samples is due to a relatively large effective mass of charge carriers. As the thermal conductivity is intrinsically low owing to the layered crystal structure and is further decreased for the Se-substituted samples because of the increased phonon scattering from point defects, the thermoelectric characteristics are promising. The highest dimensionless figure-of-merit values were seen for the $x=0.5$ sample, e.g., 0.04 at 400 K.

## 1. Introduction

A layered crystal structure with low dimensionality has been considered beneficial for a thermoelectric (TE) material with a high figure-of-merit value, $ZT=\sigma S^2T/k$, where $\sigma$ is electrical conductivity, $S$ is Seebeck coefficient, $k$ is thermal conductivity and $T$ is the operation temperature. For the layer-structured materials, high Seebeck coefficient values and low thermal conductivity values are expected because of the confinement of electrons from three-dimension to quasi-two-dimension and reduction in the phonon thermal conductivity.[1–7]

In recent years, layered ternary chromium chalcogenides of the $MCrX_2$ (M=Li, Na, K, Cu or Ag; X=S, Se) type have been attracting increasing research interest owing to their promising *ZT* values around and above room temperature, and also due to their low-temperature antiferromagnetic phase transitions ($T_N=$ 20–55 K).[8–13] The high *ZT* values in these materials derive from extremely low thermal conductivity and reasonably high electrical conductivity values. The low thermal conductivity is a result of phonon scattering by superionic anions between the $CrX_2$ layers and natural grain boundaries due to the layered structure. The superionic conduction at high temperatures indicate so-called phonon-liquid electron-crystal (PLEC) behaviour in which one of the ion constituents is dynamically disordered within an otherwise ordered crystalline framework; for such PLEC systems strong reduction in thermal conductivity is achieved, as the heat carrying phonons are extensively scattered due to the rattling of the disordered ions.[11,14,15] Owing to the PLEC state, very low lattice thermal conductivity values can be achieved at high temperatures within an electronically conductive framework.[10,12,15–20] For example for $CuCrSe_2$, *ZT* values up to 1 at 773 K have been reported.[12]

The crystal structure of $MCrX_2$ comprises $CdI_2$-type Cr-$X_2$ layers alternate with a layer of non-magnetic M atoms (M=Na, K, Cu or Ag) to give hexagonal- rhombohedral structures. The fast ion conduction in $MCrX_2$ is possible because of weakly bonded monovalent metal (M) atoms intercalated within the $CrX_2$ layers and there is a pronounced number of empty available sites between $CrX_2$ slabs.[21] Above the phase transition temperature, the $M^+$ ions drift from the occupied tetrahedral centres to other tetrahedral centres, causing a strong kinetic disorder which leads to the disturbance in phonon vibration mode, decreasing the overall thermal conductivity.[12,14,17] The phase transition temperature is significantly low (365 K) for $CuCrSe_2$, as compared to $CuCrS_2$ (675 K), $AgCrS_2$ (670 K) and $AgCrSe_2$ (474 K).[9,22–24] Also $AgCrSe_2$ has been found as a promising TE material thanks to its glass-like thermal conductivity and large Seebeck coefficient.[10,25,26]

Here we investigate the solid-solution system, $CuCr(S,Se)_2$. In this system, the two end compounds, $CuCrS_2$ and $CuCrSe_2$, are both antiferromagnets, ionic conductors, narrow-bandgap *p*-type electrical conductors, and potential TE materials. In

---

[a] *H. S. Kousar, D. Srivastava, M. Karppinen, G. C Tewari*
*Department of Chemistry and Materials Science,*
*Aalto University,*
*FI-00076 Aalto, Finland*
*E-mail: girish.tewari@aalto.fi*
*maarit.karppinen@aalto.fi*

*This article is part of a Special Collection dedicated to Professor Antoine Maignan on the occasion of his 60th birthday. Please see our homepage for more articles in the collection.*

particular, a giant room-temperature power factor value of ~2.1 mW $(m{\cdot}K)^{-2}$ was reported for $CuCrSe_2$ with a contribution of spin-orbital interaction.[6] It is also known that the TE properties of both phases are sensitive to the synthesis conditions because of their tendency for native defect formation and significant amounts of trivalent $Cr^{3+}$ ions occupying interstitial sites when the sample is sintered at high temperatures.[4–6,27,28] For example, long sintering periods at 900 °C for $CuCrS_2$,[4,6,27] or at 950–1050 °C for $CuCrSe_2$,[5,27] have been shown to enhance the TE performance. The long sintering at high temperature introduces defects in chromium sites; this increases the electrical conductivity and decreases thermal conductivity, thus enhancing the TE performance. However a recent paper reported enhanced TE properties in $CuCrS_{2-x}Se_x$ (x = 0, 0.5, 1.0, 1.5, 2) samples by replacing chalcogens and sintering and they concluded that sintering played an important role in enhancing the TE properties by decreasing the energy barriers associated with the grain boundaries.[23] However, otherwise very little is known of the electronic transport properties throughout the S/Se solid-solution range. The aim of the present work is to systematically trace the evolution of the TE transport properties with increasing x in $CuCr(S_{1-x}Se_x)_2$.

## Experimental and computational details

A series of polycrystalline $CuCr(S_{1-x}Se_x)_2$ (x = 0, 0.1, 0.2, 0.3, 0.5, 0.7, 0.8, 0.9, and 1) samples were synthesized from stoichiometric amounts of elemental precursors, Cu (99.999 %), Cr (99.0 %), S (99.999 %), and Se (99.999 %). The precursors were mixed and sealed in quartz ampoules under vacuum. The ampoules were slowly (9 °C/h) heated in a tube furnace in a step-by-step manner, such that the temperature was kept constant for 24 hours at 400 °C, 600 °C and 900 °C, and then finally slowly cooled from 900 °C to room temperature. The resultant mass was grounded to get a homogenized mixture in an argon-filled glove box, then the powders were pressed into pellets and sealed in quartz ampoules under vacuum for the second heat treatment at 900 °C for 24 h followed by slow cooling to room temperature to avoid Cu or Cr disorder.

Each sample was characterized by x-ray diffraction (XRD; PANanalytical X'Pert PRO MPD Alpha-1; Cu Kα1 radiation) for the phase purity and crystal structure determination. The low temperature TE transport properties were measured using a physical property measurement system (PPMS; Quantum Design; equipped with 9 T magnet). Electrical resistivity ($\rho$), Seebeck coefficient ($S$), and thermal conductivity ($\kappa$) were measured simultaneously by using the thermal transport option (TTO) available in the PPMS. Hall measurements were carried out using a standard four point-probe technique. In the TTO measurement, we make four linear probe connections to a rectangular shape (roughly $10\times4\times1\ mm^3$) sample along its length. A heater is attached to one end probe and two thermometers are attached to the middle probes. In isothermal condition, the heater applies heat to one end of the sample, and the temperature difference and the Seebeck voltage are measured simultaneously from the middle probes at the steady state. The Seebeck voltage is divided by the temperature difference to obtain the $S$. The $\kappa$ was estimated by using sample dimensions and the temperature difference.

The layered $MCrX_2$ compounds crystallize in a rhombohedral structure with space group R3 m. The atoms occupy 00z position with lattice translations (2/3, 1/3, 1/3) and (1/3, 2/3, 2/3) under the rhombohedral unit cell.[9] Density functional theory (DFT) calculations were performed on A-type antiferromagnetic ground state with a doubled primitive cell along the c axis. There are 24 atoms in the unit cell and the magnetic moment is assigned to $Cr^{3+}$ ions occupying hexagonal layers along the c-axis with up and down spins alternatively. The spin-polarized GGA calculations was performed using QUANTUM ESPRESSO.[29–32] The Perdew-Burke-Ernzerhof (PBE)[31] exchange correlation function was used with scalar relativistic ultrasoft pseudopotentials from GBRV (http://www.physics.rutgers.edu/gbrv/) high-throughput pseudo-potentials library. The lattice parameters were optimized using variable-cell relaxation and found to be within 2 % of the experimental value of lattice parameters. The relaxed crystal structure was used for electronic structure calculations. The plane wave cut off is kept at 60 Ryd for all the calculations. The Hellmann-Feynman forces on each atom were below 0.002 Ryd/au in the relaxed crystal structures and the total stress was below 0.25 GPa. For sampling the Brillouin zone, 11X11X1 Monkhorst–Pack grids,[20] including the 0 point were used.

## Results and discussion

From the XRD analysis, all the $CuCr(S_{1-x}Se_x)_2$ samples were found to consist of a single rhombohedral (space group R3 m) phase, as expected. Figure 1(a) shows the diffraction patterns, and Figure 1(b) depicts the lattice parameters as a function of x for the samples. With increasing x the lattice parameters linearly increase according to Vegard's law,[33] indicating the complete solid solubility of the S and Se atoms.

The electronic band-structure calculations for the three compositions of $CuCrS_2$, CuCrSSe and $CuCrSe_2$ (assuming A-type antiferromagnetic ordering) are presented in Figure 2. For the $CuCrS_2$ and CuCrSSe phases, four extrema are seen in their valence bands: two near A symmetric point along Q(AH) and R(AL) symmetry lines, and two near $\Gamma$ symmetric point along $\Sigma(\Gamma M)$ and $\Lambda(\Gamma K)$ symmetry lines, see Figures 2(a) and (b). All the extrema have nearly identical energies, although the extrema located on $Q(\Sigma)$ symmetry line has slighly higher energy than the others. Therefore, the valence band maxima (VBM) for $CuCrS_2$ and CuCrSSe appear along $Q(\Sigma)$ symmetry line. For $CuCrSe_2$, the VBM is situated at $\Gamma$ points, see Figure 2(c). Two very close conduction band minima (CBM) are situated in between A–H and $\Gamma$-K lines for all the three phases.

The total and partial electronic density of states (PEDOS) for each phase are shown on the corresponding right panels in Figure 2. The valence band is dominated by 3*d* orbitals of Cu and Cr1 and *p* orbitals of S and Se for all the phases. The contribution from *p* orbitals increases for the Se substituted phases near the Fermi level indicating an enhancement in hole density. This might be due to the stronger hybridization between the *d* states of Cr1 and the *p* states of S or Se. The conduction band is dominated by 3*d* orbitals of Cr1 and Cr2 with mixing of *p* orbitlas of S and Se. The Cu 3*d* orbital does not contribute to the conduction band, and consequently the PEDOS indicates the +1 oxidation state for Cu. The strong contribution of the *p* orbitals of S and Se in valence band clearly suggests that by controlling the Se-for-S substitution level it

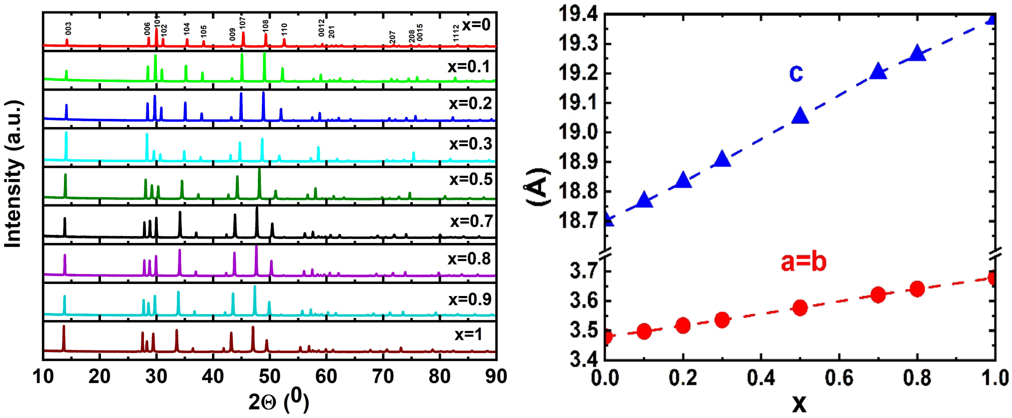

**Figure 1.** (a) XRD patterns for the $CuCr(S_{1-x}Se_x)_2$ samples; (b) lattice parameters plotted against the Se content x.

could be possible to tune the electrical transport properties in these compounds.

From the computational analysis, the three phases of $CuCrS_2$, CuCrSSe and $CuCrSe_2$ appear as narrow-band semiconductors with the indirect bandgap at 0.42, 0.30 and 0.10 eV, respectively. Owing to the multiple valleys, these compounds can be termed as multi-valley semiconductors. It should be mentioned that the results obtained here for the two end members, $CuCrS_2$ and $CuCrSe_2$, are in agreement with those previously reported for these compositions.[27,28] The effective magnetic moment on Cr atoms was calculated to be 3.28 $\mu_B$, 3.37 $\mu_B$, and 3.50 $\mu_B$ for $CuCrS_2$, CuCrSSe and $CuCrSe_2$, respectively. The lower value of numerically calculated local magnetic moment in comparison to the expetcted value of 3.9 $\mu_B$ for $Cr^{3+}$ with frozen orbital component may be attributed to strong hybridization of the Cr 3*d* orbital with the *p* orbitals of surrounding chalcogen atoms.

Hall effect measurements were carried out for selected $CuCr(S_{1-x}Se_x)_2$ samples to identify the type and density of charge carriers at different temperatures. In Figures 3(a) and 3(b), we present the Hall resistance ($R_{xy}$) versus magnetic field (B) isotherms for the $x=0$ and 0.5 samples. The temperature dependence of Hall coefficient ($R_H$) and charge carrier density ($n$) data for $x=0$, 0.2, 0.5 and 0.8 are shown in Figures 3(c) and 3(d), respectively. The data clearly reveal the *p*-type behaviour of charge carriers for all the studied samples. For $x=0$ from Figures 3(c) and 3(d), the temperature dependences of $R_H$ and $n$ are typical for semiconducting behaviour, as $R_H$ decreases and $n$ increases rapidly with temperature; at 300 K, $n$ is $4.67\times 10^{15}$ $cm^{-3}$ for this sample. Increasing the Se content results in a sharp increase in $n$: for the $x=0.2$ and 0.5 samples, the 300-K $n$ values are $4.94\times 10^{19}$ $cm^{-3}$ and $2.89\times 10^{20}$ $cm^{-3}$, respectively; these values are essentially similar to those reported earlier.[34] The systematic increase in charge carrier density with increasing x is in line with our computational results showing a decrease in electronic bandgap with increasing Se-for-S substitution level. However, further increase in the Se content beyond $x=0.5$ did not significantly increase $n$. Interestingly, the $R_H$ and $n$ values for the Se-containing samples hardly change with temperature. This behaviour is very similar to degenerate semiconductors or metals.

Thermoelectric transport property measurement data for the samples are presented in Figure 4. From the temperature dependence of electrical resistivity data (Figure 4(a)), the $x=0$ sample is clearly semiconducting, as $\rho$ decreases with temperature; activation energy obtained by linearly fitting the high temperature region using the Arrhenius equation (*Ln*($\rho$) vs. *1/T*) is 0.21 eV. This significantly lower activation energy value in comparison to the computationally calculated electronic bandgap value of 0.42 eV could be related to the formation of chromium defects.[4–6,24]

In case of the Se-for-S substituted samples the resistivity decreases with increasing x due to increase in charge carrier density, see Figure 3(d). With increasing Se content, also a semiconductor-to-metal transition is seen for $x>0.5$. The temperature dependence of resistivity for those metallic phases indicates that $\rho$ remains high (in the range of 1–3 mΩ-cm) even at the lowest temperature of measurement (2 K), and increases slowly with temperature. These observations point towards heavily doped or degenerate semiconductors.

From the Seebeck coefficient versus temperature plots presented in Figure 4(b), the 300-K $S$ value for the $x=0$ sample is 690 μV/K. With increasing x, the $S$ value systematically decreases. This is related to the increased charge carrier density with increasing selenium content. The $n$ and $S$ values are related through a simple model of electron transport, as for metals or degenerate semiconductors $S$ depends on $n$ in parabolic band and energy-independent scattering approximation is given by:

$$S(T) = \frac{8\pi^2 k_B^2}{3eh^2} m^* T \left(\frac{\pi}{3n}\right)^{2/3}$$

where $n$ is density and $m^*$ is the effective mass of charge carriers. In our samples except the $CuCrS_2$ ($x=0$) phase, $n$ roughly remains constant with temperature, see Figure 3(d). Hence, we can fit $S(T)$ versus $T$ with a linear dependence at high temperature, as shown with the dashed black lines in the

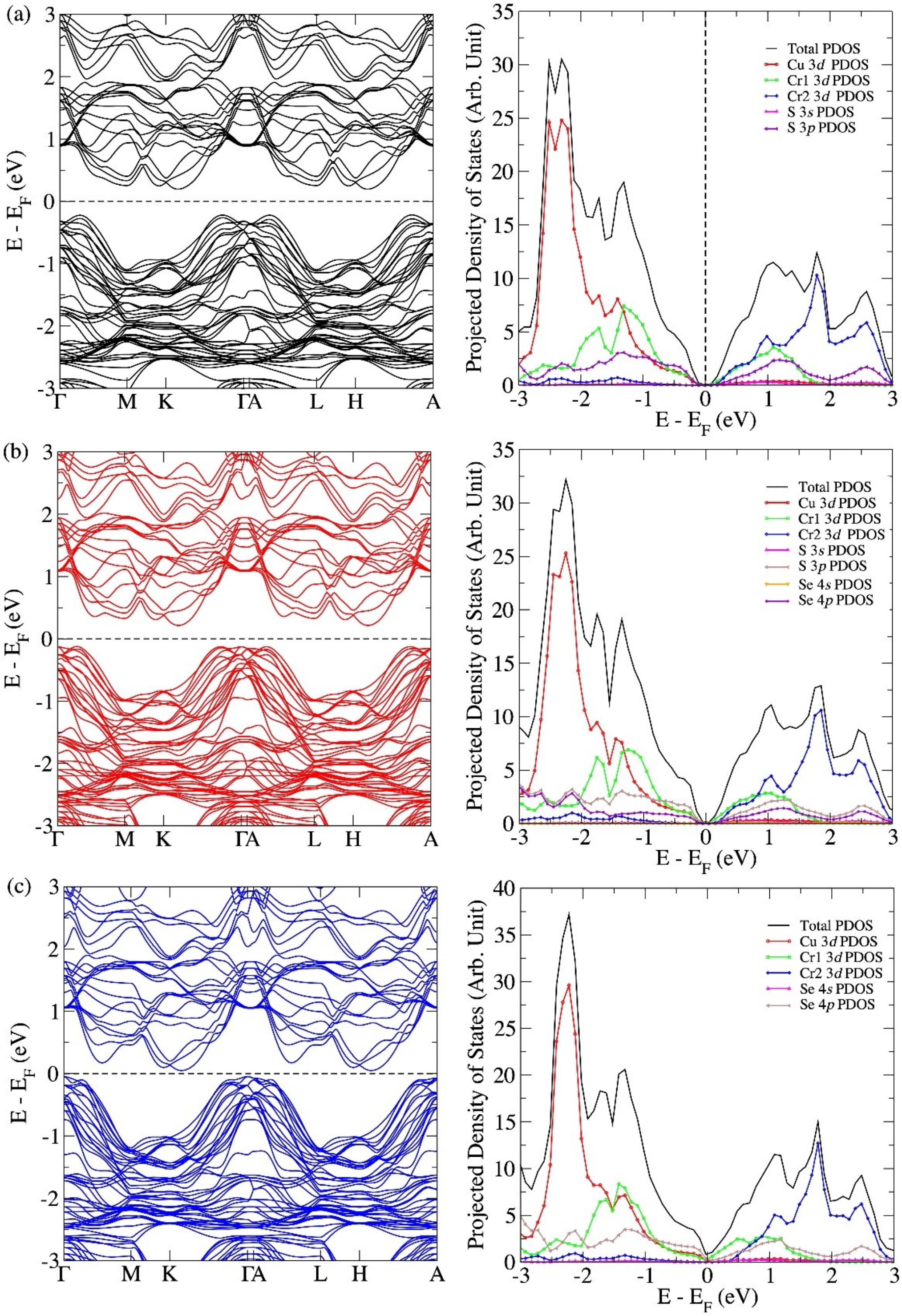

**Figure 2.** Spin-polarized DFT calculated energy band structure and corresponding PDOS for A-type antiferromagnetic (a) $CuCrS_2$, (b) CuCrSSe, and (c) $CuCrSe_2$. Note: electronic band structure and total EDOS and PEDOS are identical for both spin directions.

figure. The slope of the best linear fit could be used to find the effective mass of charge carriers. We used the value of $n$ at 300 K to estimate the $m^*$ values, which for the Se-containing samples were found significantly large and increasing with x: e.g. 1.04 $m_0$ for x = 0.1 and 2.90 $m_0$ for x = 0.5. The large value of $m^*$ is in line with the large $S$ values observed for the Se-containing samples.

The temperature dependence of thermal conductivity data (total $\kappa$) for the samples are presented in Figure 4(c). At 300 K, the x = 0 sample shows a relatively high $\kappa$ value of 1.35 W/K-m

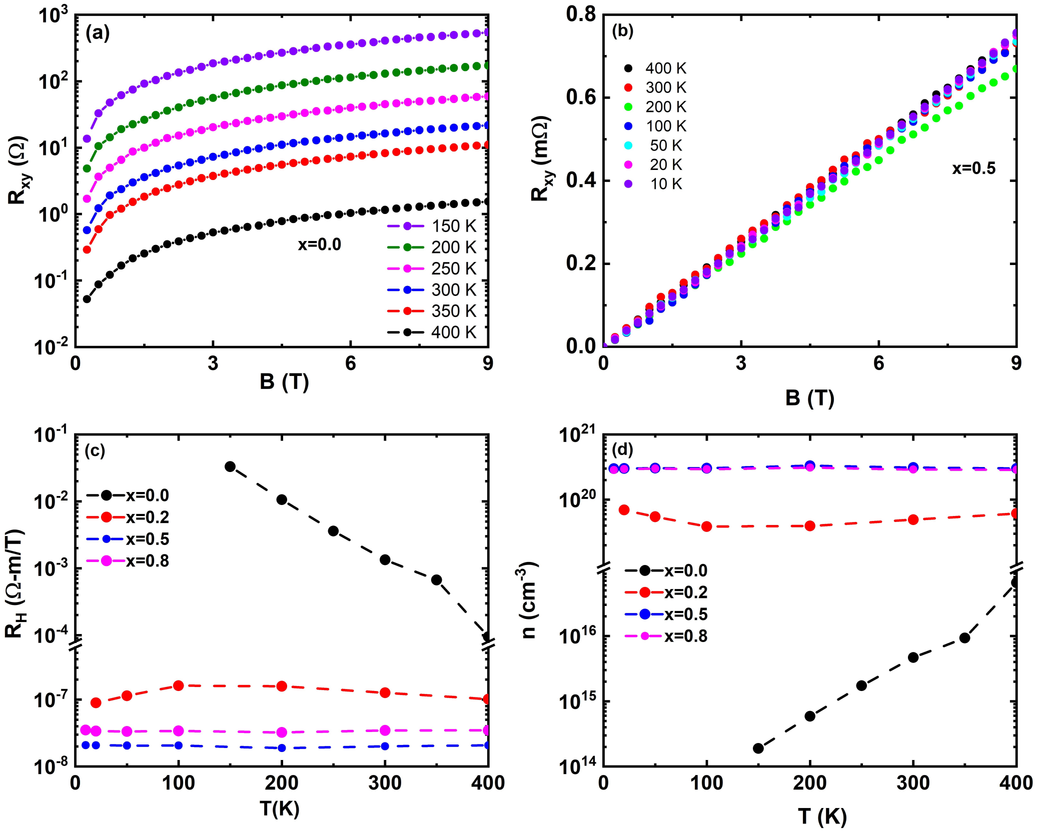

**Figure 3.** Hall effect measurement results for the CuCr($S_{1-x}Se_x$)$_2$ samples: Hall resistance versus magnetic isotherms at different temperatures for (a) x = 0, and (b) x = 0.5; (c) temperature dependence of (c) Hall coefficient, and (d) charge carrier density for representative samples.

in comparison to previously reported studies.[4,5,35] The $\kappa$ decreases with Se-substitution level, reaching the minimum value of 0.84 W/K-m for x = 0.5. This is probably related to a rise in phonon scattering due to distortion in lattice due to S/Se mixing. Further increase in x resulted in increased $\kappa$ values for the x = 0.8, 0.9 and 1 samples, owing to an increase in electronic contribution due to the higher charge carrier density.

Finally, we present the *ZT* values for all the samples in Figure 4(d) and summarize the data in Table 1. The *ZT* for $CuCrS_2$ remains negligible in the temperature range from 300 to 400 K, but increases rapidly with increasing Se content x, reaching the highest value at 0.049 for x = 0.5 at 400 K. The strong rise in *ZT* at 400 K is primarily due to the increased electrical conductivity and reduced thermal conductivity.

To discuss the behavior of thermal conductivity in more detail we consider the electronic thermal conductivity ($\kappa_e$) and lattice thermal conductivity ($\kappa_l$) contributions of the total thermal conductivity $\kappa = \kappa_e + \kappa_l$ separately. The $\kappa_e$ can be estimated based on the Wiedemann – Franz law: $\kappa_e = {}^{LT}/_{\rho}$, where L is the Lorenz number. Among the present samples, the thus calculated $\kappa_e$ values presented in Figure 5(a), account for less than 15 % of the total $\kappa$ value at 400 K in case of the most conducting samples of x = 0.9 and 1. The $\kappa_l$ values deduced by subtracting $\kappa_e$ from total $\kappa$ are presented in Figure 5(b). This

**Table 1.** Thermoelectric transport properties measured at 300 K for the CuCr($S_{1-x}Se_x$)$_2$ samples; also given are, activation energy values calculated using Arrhenius equation and electronic bandgap values calculated using spin-polarized DFT.

| Sample | *n* (*cm*$^{-3}$) | Act. ener. (eV) | *Bandgap* (eV) | $\rho$ (mΩ-cm) | *S* (μV/K) | *K* (W/K-*m*) | *ZT* |
|---|---|---|---|---|---|---|---|
| x = 0.0 | 4.67x$10^{15}$ | 0.21 | 0.42 | 5.72 × $10^6$ | 689 | 2.13 | – |
| x = 0.2 | 4.9x$10^{19}$ | – | – | 27.6 | 192 | 1.09 | 0.036 |
| x = 0.5 | 2.8x$10^{20}$ | metal | 0.30 | 13.6 | 122 | 0.81 | 0.040 |
| x = 0.8 | 3.11x$10^{20}$ | metal | – | 4.77 | 75 | 1.55 | 0.025 |
| x = 0.9 | 4.12x$10^{20}$ | metal | – | 2.46 | 57 | 1.42 | 0.031 |
| x = 1.0 | 4.25x$10^{20}$ | metal | 0.10 | 2.45 | 42 | 2.32 | 0.022 |

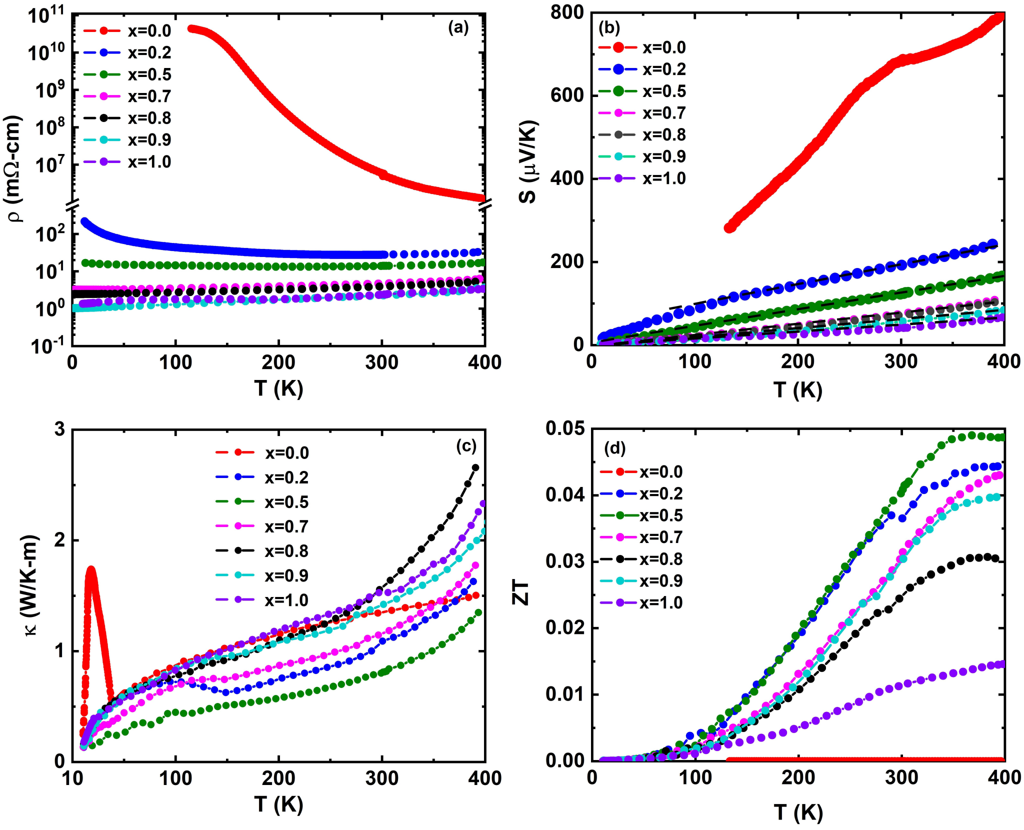

**Figure 4.** Thermoelectric characterization results for the $CuCr(S_{1-x}Se_x)_2$ samples: (a) electrical resistivity, (b) Seebeck coefficient, (c) thermal conductivity, and (d) figure-of-merit versus temperature.

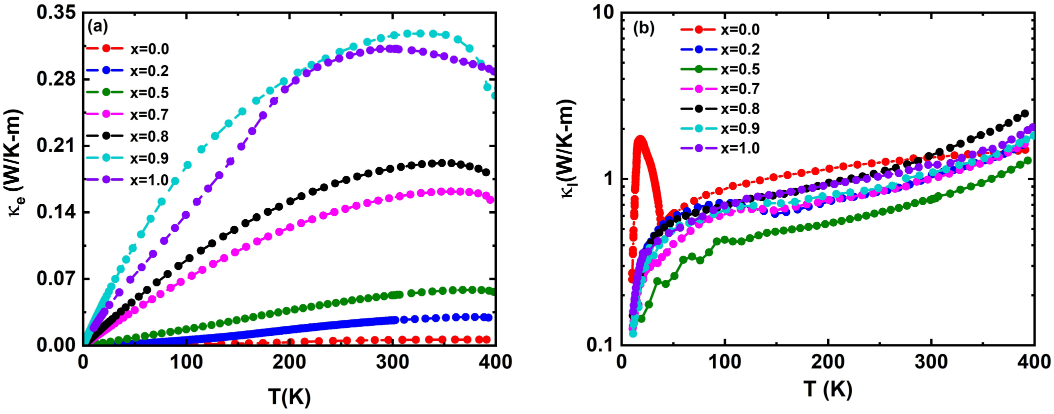

**Figure 5.** (a) Electronic, and (b) lattice contributions of thermal conductivity for the $CuCr(S_{1-x}Se_x)_2$ samples.

clearly suggests that $\kappa_l$ dominates the thermal conductivity in these materials. For $CuCrS_2$ ($x=0$), $\kappa_l$ rapidly increases with temperature and shows a peak near 18 K followed by a sharp decrease till 40 K. The sharp change in $\kappa_l$ below 40 K is obviously due to the structural phase transition from rhombohedral to monoclinic structure accompanied with the antiferromagnetic transition, and unusually large magnetoelastic coupling in $CuCrS_2$ that is supposed to be a nature of first-order magnetic transition.[36–39] The magnetoelastic coupling results in strong scattering of phonons by short-range magnetic correlations. The $\kappa_l$ increases slowly with temperature in the paramagnetic phase above 40 K. In contrast, all the Se-containing samples show significantly lower $\kappa_l$ values compared to $CuCrS_2$ below the antiferromagnetic transition at 40 K. However above 40 K with increasing Se content, $\kappa_l$ decreases for samples up to $x=0.5$ and then increases again with further increase in the Se content. This clearly shows the decrease in $\kappa_l$ with Se substitution is related to scattering of phonons due to enhancement of point-defects. The low-temperature sharp peak observed for $CuCrS_2$ quickly disappears when Se is introduced in the samples; instead, we observe initially a slow increase in $\kappa$ for x = 0.2, 0.5 and 0.7, passing through a shallow maximum around 100 K with a further increasing behavior at high temperatures. For the $x > 0.7$ samples, $\kappa_l$ continuously increases with temperature with different exponent in different regions. The $\kappa_l$ roughly follows the $T^{1.5}$ behavior up to 25 K and the $T^{0.5}$ behavior until 300 K for these samples. This behavior of $\kappa_l$ in these layered materials is typical for disordered semiconductors or bulk metallic glasses where the resonant scattering (phonon-grain boundary, phonon-defect, and phonon-phonon scattering) of phonons at low temperature causes localization of phonons and results in hopping conduction of phonons and roughly obeys linear $T$ dependance.[40] The disappearance of the sharp change in $\kappa_l$ at low temperatures about the magnetic transition signifies the absence of structural phase transition in Se-containing samples.

## Conclusions

We have investigated the low-temperature thermoelectric transport properties of the layered copper chromium chalcogenides thorough the entire solid-solution range of $CuCr(S_{1-x}Se_x)_2$ from x = 0 to 1. We also studied the spin-polarized electronic band structures for A-type antiferromagnetic $CuCrS_2$, CuCrSSe and $CuCrSe_2$ compositions. The band structure results showed narrow-band semiconducting behaviour for these phases, with a decreasing bandgap (from 0.42 to 0.10 eV) with increasing Se-for-S substitution level. Experimentally, a semiconductor-to-metal transition was seen with increasing x.

A large Seebeck coefficient was found for the semiconducting $CuCrS_2$ at 300 K, and it remained high for the metallic Se-containing samples as well, owing to the large effective mass of charge carriers. Moreover, thermal conductivity was found appreciably low for these samples owing to the layered crystal structure; it got further reduced with the Se-for-S substitution due to increased phonon scattering from point defects. Accordingly, the thermoelectric figure-of-merit was maximized for the x = 0.5 sample; the $ZT$ value for this sample at 400 K was around 0.049.

## Acknowledgements

HSK would like to acknowledge Jenny Ja Antti Wihuri foundation for research grant (2021-2023). The authors would also like to acknowledge Academy of Finland (Profi3 and PREIN). This work made use of the RawMatters Finland infrastructure (RAMI) facilities at Aalto University.

## Conflict of Interest

The authors declare no conflict of interest.

## Data Availability Statement

The data that support the findings of this study are available on request from the corresponding author. The data are not publicly available due to privacy or ethical restrictions.

[1] L. D. Hicks, M. S. Dresselhaus, *Physucal Rev. B* **1993**, *47*, 12727–12731.
[2] A. Maignan, E. Guilmeau, F. Gascoin, Y. Bréard, V. Hardy, *Sci. Technol. Adv. Mater.* **2012**, *13*, DOI 10.1088/1468-6996/13/5/053003.
[3] Y. Kinemuchi, E. Guilmeau, O. I. Lebedev, A. Maignan, *J. Appl. Phys.* **2011**, *110*, DOI 10.1063/1.3669392.
[4] G. C. Tewari, T. S. Tripathi, P. Kumar, A. K. Rastogi, S. K. Pasha, G. Gupta, *J. Electron. Mater.* **2011**, *40*, 2368–2373.
[5] G. C. Tewari, T. S. Tripathi, H. Yamauchi, M. Karppinen, *Mater. Chem. Phys.* **2014**, *145*, 156–161.
[6] G. C. Tewari, T. S. Tripathi, A. K. Rastogi, *Z. Kristallogr.* **2010**, *225*, 471–474.
[7] Y. Zhou, L. D. Zhao, *Adv. Mater.* **2017**, *29*, DOI 10.1002/adma.201702676.
[8] P. F. Bongners, C. F. Van Bruggen, J. Koopstra, F. A. M. Omloo, G. A. Wiegers, F. Jellinek, **1968**, *29*, 977–984.
[9] F. M. R. Engelsman, G. A. Wiegers, F. Jellinek, B. Van Laar, *J. Solid State Chem.* **1973**, *6*, 574–582.
[10] F. Gascoin, A. Maignan, *Chem. Mater.* **2011**, *23*, 2510–2513.
[11] M. Beekman, D. T. Morelli, G. S. Nolas, *Nat. Mater.* **2015**, *14*, 1182–1185.
[12] S. Bhattacharya, R. Basu, R. Bhatt, S. Pitale, A. Singh, D. K. Aswal, S. K. Gupta, M. Navaneethan, Y. Hayakawa, *J. Mater. Chem. A* **2013**, *1*, 11289–11294.
[13] D. Beretta, N. Neophytou, J. M. Hodges, M. G. Kanatzidis, D. Narducci, M. Martin-Gonzalez, M. Beekman, B. Balke, G. Cerretti, W. Tremel, A. Zevalkink, A. I. Hofmann, C. Müller, B. Dörling, M. Campoy-Quiles, M. Caironi, *Mater. Sci. Eng. R* **2019**, *138*, 210–255.
[14] J. L. Niedziela, D. Bansal, A. F. May, J. Ding, T. Lanigan-Atkins, G. Ehlers, D. L. Abernathy, A. Said, O. Delaire, *Nat. Phys.* **2019**, *15*, 73–78.
[15] H. Liu, X. Shi, F. Xu, L. Zhang, W. Zhang, L. Chen, Q. Li, C. Uher, T. Day, G. Snyder Jeffrey, *Nat. Mater.* **2012**, *11*, 422–425.
[16] Y. Qin, Y. Xiao, L. D. Zhao, *APL Mater.* **2020**, *8*, DOI 10.1063/1.5144097.
[17] A. Gagor, D. Gnida, A. Pietraszko, *Mater. Chem. Phys.* **2014**, *146*, 283–288.
[18] R. A. Yakshibayev, V. N. Zabolotsky, R. F. Almukhametov, *Solid State Ionics* **1988**, *31*, 1–4.
[19] D. J. Voneshen, H. C. Walker, K. Refson, J. P. Goff, *Phys. Rev. Lett.* **2017**, *118*, DOI 10.1103/PhysRevLett.118.145901.
[20] B. Li, H. Wang, Y. Kawakita, Q. Zhang, M. Feygenson, H. L. Yu, D. Wu, K. Ohara, T. Kikuchi, K. Shibata, T. Yamada, X. K. Ning, Y. Chen, J. Q. He, D. Vaknin, R. Q. Wu, K. Nakajima, M. G. Kanatzidis, *Nat. Mater.* **2018**, *17*, 226–230.
[21] B. A. Boukamp, G. A. Wiegers, *Solid State Ionics* **1983**, *9–10*, 1193–1196.
[22] F. Damay, S. Petit, M. Braendlein, S. Rols, J. Ollivier, C. Martin, A. Maignan, *Phys. Rev. B: Condens. Matter Mater. Phys.* **2013**, *87*, DOI 10.1103/PhysRevB.87.134413.
[23] A. I. Romanenko, G. E. Chebanova, I. N. Katamanin, M. V. Drozhzhin, S. B. Artemkina, M.-K. Han, S.-J. Kim, H. Wang, *J. Phys. D* **2022**, *55*, DOI 10.1088/1361-6463/ac453e.
[24] R. A. Yakshibaev, G. R. Akmanova, R. F. Almukhametov, V. N. Konev, *Phys. Status Solidi* **1991**, *124*, 417–426.
[25] A. Maignan, E. Guilmeau, F. Gascoin, Y. Bréard, V. Hardy, *Sci. Technol. Adv. Mater.* **2012**, *13*.

[26] F. Damay, S. Petit, S. Rols, M. Braendlein, R. Daou, E. Elkaïm, F. Fauth, F. Gascoin, C. Martin, A. Maignan, *Sci. Rep.* **2016**, *6*, DOI 10.1038/srep23415.

[27] D. Srivastava, G. C. Tewari, M. Karppinen, *J. Phys. Condens. Matter* **2014**, *26*, DOI 10.1088/0953-8984/26/50/505501.

[28] D. Srivastava, G. C. Tewari, M. Karppinen, R. M. Nieminen, *J. Phys. Condens. Matter* **2013**, *25*, DOI 10.1088/0953-8984/25/10/105504.

[29] S. P. Giannozzi, N. B. Baroni, M. Calandra, R. Car, I. C. Cavazzon, D. Ceresoli, G. L. Chiarotti, M. Cococcioni, I. Dabo, A. D. Corso, S. De Gironcoli, S. Fabris, G. Fratesi, R. Gebauer, U. Gerstmann, C. Gougoussis, A. Kokalj, M. Lazzeri, L. Martin-Samos, N. Marzari, F. Mauri, R. Mazzarello, S. Paolini, A. Pasquarello, L. Paulatto, C. Sbraccia, S. Scandolo, G. Sclauzero, A. P. Seitsonen, A. Smogunov, P. Umari, R. M. Wentzcovitch, *J. Phys. Condens. Matter* **2017**, *29*, DOI 10.1088/1361-648X/aa8f79.

[30] P. Giannozzi, T. O. Andreussi, O. B. Brumme, M. B. Nardelli, M. Calandra, R. Car, C. Cavazzoni, D. Ceresoli, M. Cococcioni, N. Colonna, I. Carnimeo, A. D. Corso, S. De Gironcoli, P. Delugas, R. A. Distasio, A. Ferretti, A. Floris, G. Fratesi, G. Fugallo, R. Gebauer, U. Gerstmann, F. Giustino, T. Gorni, J. Jia, M. Kawamura, H.-Y. Ko, A. Kokalj, E. Küçükbenli, M. Lazzeri, M. Marsili, N. Marzari, F. Mauri, N. L. Nguyen, H.-V. Nguyen, A. Otero-De–La-Roza, L. Paulatto, D. R. S. Poncé, R. Sabatini, B. Santra, M. Schlipf, A. P. Seitsonen, A. Smogunov, I. Timrov, T. Thonhauser, P. Umari, N. Vast, X. Wu, S. Baroni, *J. Phys. Condens. Matter* **2009**, *21*, DOI http://iopscience.iop.org/0953-8984/21/39/395502/.

[31] J. P. Perdew, K. Burke, M. Ernzerhof, *Phys. Rev. Lett.* **1996**, *77*, 3865–3868.

[32] G. K. H. Madsen, J. Carrete, M. J. Verstraete, *Comput. Phys. Commun.* **2018**, *231*, 140–145.

[33] K. T. Jacob, S. Raj, L. Rannesh, *Int. J. Mater. Res.* **2007**, *98*, 776–779.

[34] G. C. Tewari, M. Karppinen, A. K. Rastogi, *J. Solid State Chem.* **2013**, *198*, 108–113.

[35] G. C. Tewari, T. S. Tripathi, A. K. Rastogi, *J. Electron. Mater.* **2010**, *39*, 1133–1139.

[36] J. C. E. Rasch, M. Boehm, C. Ritter, H. Mutka, J. Schefer, L. Keller, G. M. Abramova, A. Cervellino, J. F. Löffler, *Phys. Rev. B* **2009**, *80*, DOI 10.1103/PhysRevB.80.104431.

[37] A. Karmakar, K. Dey, S. Chatterjee, S. Majumdar, S. Giri, *Appl. Phys. Lett.* **2014**, *104*, DOI 10.1063/1.4863937.

[38] F. Damay, C. Martin, V. Hardy, G. Andr, S. Petit, A. Maignan, *Phys. Rev. B* **2011**, *83*, DOI 10.1103/PhysRevB.83.184413.

[39] N. Tsujii, H. Kitazawa, *J. Phys. Condens. Matter* **2007**, *19*, DOI 10.1088/0953-8984/19/14/145245.

[40] Z. Zhou, C. Uher, D. Xu, W. L. Johnson, W. Gannon, M. C. Aronson, *Appl. Phys. Lett.* **2006**, *89*, DOI 10.1063/1.2234281.

Manuscript received: April 19, 2023
Revised manuscript received: May 23, 2023
Accepted manuscript online: June 8, 2023